RSC Advances

Biocompatible hyperbranched epoxy/silver-reduced graphene oxide-curcumin nanocomposite as an advanced antimicrobial material

Shaswat Barua, Pronobesh Chattopadhyay, Mayur M. Phukan, Bolin K .Konwar, Johirul Islam and Niranjan Karak*
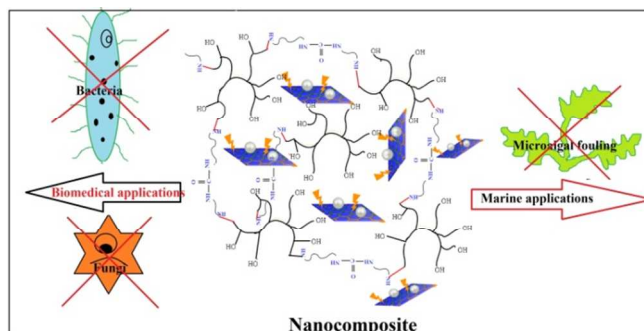
Hyperbranched epoxy/silver reduced graphene oxide immobilized curcumin nanocomposite as an antimicrobial material

ARTICLE TYPE

Biocompatible hyperbranched epoxy/silver-reduced graphene oxide-curcumin nanocomposite as an advanced antimicrobial material

Shaswat Barua[a], Pronobesh Chattopadhyay[b], Mayur M. Phukan[c], Bolin K .Konwar[c], Johirul Islam[b] and Niranjan Karak[a]*

Fouling due to bacteria, fungi and algae is a serious problem in the domains of biomedical research, paints and coatings. Toxicity of the prevailing antimicrobial systems demands benign materials with adequate antimicrobial properties. In this context, thermosetting hyperbranched epoxy/silver-reduced graphene oxide-curcumin nanocomposites with antimicrobial attributes against bacteria, fungi and algae are reported here for the first time. The nanocomposite also exhibited high mechanical properties with tensile strength: 54-65 MPa and elongation at break: 17-21%. Ultrasonication, the 'green' tool was used to immobilize curcumin onto the silver-reduced graphene oxide nanohybrid. The nanocomposites inhibited the growth of *Staphylococcus aureus* and *Candida albicans*, the microorganisms found in surgical infection sites, with minimum inhibitory concentrations of 38 and 41 µg/mL at 3% loading of the immobilized nanohybrid. Further, the nanocomposite prevented the growth of the green microalgae *Chlorella* sp. Moreover, *in vitro* and *in vivo* bio-assays confirmed the biocompatibility of the prepared nanocomposite. This study endorses the nanocomposite as an efficient antimicrobial material for different advanced applications from biomedical domain to marine coatings.

Introduction

Microbial biofouling is a serious problem associated with biomedical devices, implants, marine coatings, food packaging materials etc. Formation of microbial biofilms over biomedical devices and implants causes severe infections at surgical sites[1] Again, surfaces that are regularly in contact with the aquatic environment are vulnerable to the growth of marine algae, microorganisms etc. which cause severe crisis in the marine industry. Hence, it needs proper attention for finding a suitable way to address such problems. Antimicrobial thin films and surfaces with differential properties have been designed to sort out the abovementioned inconvenience.[2-4] Use of metals in such thin film applications has been preferred till the last decade.[5,6] But, induction of toxicity to the non-target organisms restricted their uses.

On the contrary, biocompatible metal nanoparticles based thin film with efficient antimicrobial activity may be a good alternative to the conventionally used systems. Silver is a competent candidate in this regard. Efficiency of silver nanoparticles (AgNP) against different bacteria and fungi is well reported in literature.[7-10] Interestingly, AgNP prepared via 'greener' routes were found to be compatible with the bio- and eco-systems.[7] However, incorporation of metal nanoparticles into a polymeric system rarely contributes to the mechanical strength of the system.[11] Thus, carbon based nanomaterials, like graphene may be considered to enjoy the twin goals of efficient antimicrobial properties and high mechanical attributes. Moreover, graphene-based nanomaterials have already proven their importance in the fields of nanomedicine, catalysis, electronics etc.[12] Recently, we designed a nanohybrid of same stature by simultaneous reduction of graphene oxide and silver salt.[13] The resulted reduced graphene oxide-silver nanohybrid (Ag-RGO) showed efficient antimicrobial activity and excellent biocompatibility. Immobilization of a bio-molecule like curcumin is further expected to enhance such activities in the system (Ag-RGO-Cur). Curcumin is a traditionally known molecule of turmeric (*Curcuma longa*), a natural preservative and ingredient of common food items that possesses tremendous antimicrobial activity.[14] Hence, it was planned to immobilize onto the aforementioned nanohybrid to prepare an antimicrobial material. Again, epoxy is extensively used by the thin film industries as a binder.[15] Hyperbranched epoxy proved its superiority over the conventionally used linear one.[16,17] Researchers witnessed improvement of thermo-mechanical properties of hyperbranched epoxy upon formation of nanocomposites with different nanomaterials such as clay, metal nanoparticles etc.[18-20] However, graphene based hyperbranched epoxy nanocomposites are rare in literature.[21,22] The proposed work urges upon the preparation of a multifunctional nanocomposite material, which would be useful for advanced antimicrobial applications. Biocompatibility of the

nanocomposites would be significantly considered during the study.

The overall study put forward a hyperbranched epoxy/Ag-RGO-Cur nanocomposite as an advanced material, which is expected to be useful in biomedical and marine applications.

Experimental

Materials

The hyperbranched epoxy resin was prepared by reacting glycerol and bisphenol A with epichlorohydrin according to our recently reported protocol.[16] Graphite flakes with 99% purity (Loba Chemie, India) and AgNO$_3$ (Qualigens®, India) were used as obtained. Turmeric (*C. longa*) was collected from Tezpur University (Assam, India) campus.

Extraction of curcumin

Turmeric was sun dried and ground to powder. Curcumin was extracted from 25 g of turmeric powder using solvent (toluene) extraction technique.[23] The obtained curcumin was dried at room temperature.

Preparation of Ag-RGO-Cur

Ag-RGO was prepared by following our recently reported method.[13] In brief, Hummer's method was employed to produce graphene oxide (GO) from graphite.[24] GO (500 mg) was dispersed in 100 mL of water using ultrasonication for about 20 min. Then, *Colocasia esculenta* leaf extract was added into the above dispersion and stirred for 10 min. AgNO$_3$ solution (0.03 M) was added to the abovementioned mixture and again stirred for 8 h at room temperature. Ag-RGO settled down after completion of the reaction. This was washed successively by centrifugation and kept in a vacuum oven for drying.

Ag-RGO (0.5 g) was dispersed in 15 mL tetrahydrofuran (THF, SD fine Chem., India) by sonicating it for 15 min. An amount of 0.25 g of curcumin was dissolved separately in 5 mL of THF and added to the above dispersion. The dispersion was stirred at room temperature for 4 h, followed by 30 min of ultrasonication (amplitude: 60% and cycles: 0.5). It was then centrifuged for 15 min at 1006×g (3000 rpm) and the supernatant (in THF) was discarded. The process was repeated to discard the undesired components. The immobilized system (Ag-RGO-Cur) was collected and allowed to dry at room temperature.

Preparation of the nanocomposites

Ag-RGO-Cur was dispersed in THF and incorporated into the hyperbranched epoxy resin in 1, 2 and 3 wt% separately. The mixture was stirred at 50 °C for 4 h. Then, it was ultrasonicated for 15 min in each case under the same conditions as stated earlier. Prepared nanocomposites were coded as HGGS1, HGGS2 and HGGS3 for 1, 2 and 3 wt% of Ag-RGO-Cur respectively.

Curing study

Crosslinking of the nanocomposites was done by mixing them with poly(amido amine) (equimolar to the epoxy equivalent of the resin). The mixture was hand stirred and cast onto steel plates (150 mm x 100 mm x 1.44 mm). The steel plates were kept under ambient conditions for escaping of the volatiles. After the plates became touch free, they were cured in an oven at specified temperatures. Crosslinking percentage was calculated by noting the swelling of the films (in THF).[16]

Characterization

The UV-visible spectra of the nanohybrid and the nanocomposites were taken in a Hitachi, U-2001, Tokyo, Japan spectrophotometer. FTIR spectra were taken by an Impact-410, Nicolet, USA spectrophotometer. Patterns of X-ray diffraction for the nanocomposites were recorded in a 'Miniflex' X-ray diffractometer (Rigaku Corporation, Japan) over a scanning range of 2θ = 10-70°, at 2.0° min^{-1} scanning rate. Morphology and distribution of the nanohybrid inside the hyperbranched epoxy matrix was scrutinized with the help of a transmission electron microscope (TEM, JEOL-JEM 2100) at an operating voltage of 200 kV. Mechanical strength, elongation at break and lap sheer tensile adhesive strength of the thermosetting nanocomposites were determined by a Universal Testing Machine (UTM, WDW10, Jinan, China, load cell=10 kN, with a crosshead speed of 50 mm/min). For the tensile strength test rectangular films were taken with dimension of 60 × 10 × 0.3 mm^3. Overlapping wood surfaces (25 × 25 × 0.3 mm^3) were prepared by applying the nanocomposites at the interfaces for determining the lap-shear tensile adhesive strength . Scratch hardness of the thermosets was recorded by a scratch hardness tester (Model no. 705, Sheen, UK) associated with a stylus accessory (ASTM G171). Impact strength was tested by standard falling weight (ball) method (ASTM D 1709) in an Impact tester (S. C. Dey). A mandrel with diameter 1-100 mm was used to test the bending of the nanocomposites (standard ASTM D 522). All the tests were performed in triplicates and average values were considered.

Release of Ag-RGO-Cur

Release profile of Ag-RGO-Cur was assayed by immerging HGGS3 films (1 cm× 1 cm) in phosphate buffer saline (PBS, pH: 7.4) at physiological temperature (37 °C, under shaking condition, 100 rpm). Similarly, an artificial sea-water (ASW) system was used (prepared according to a reported method[25]) to examine the release of Ag-RGO-Cur (at room temperature, ca. 25 °C under shaking condition, 100 rpm). At specified immersion times ranging from 0 and 7 days (0-168 h), 1 mL of the aliquot was withdrawn, followed by refilling of same amount of the fresh medium. Absorbance was analyzed at λ_{max} 418 nm in a UV-visible spectrophotometer (Hitachi, U-2001, Tokyo, Japan). Cumulative release (percentage, w/w) of the components was calculated from the obtained data with the help of standard curves of Ag-RGO-Cur in PBS and ASW. Obtained data were presented here as mean±SD from the triplicate results.[26]

Antimicrobial activity against bacteria, fungi and algae

Microbial adhesion and proliferation in surgical sites lead to severe infections, which may be life demanding. To protect medical appliances and implants from such infection, protective antimicrobial coatings are used. *Staphylococcus aureus* (ATCC 11632) and *Candida albicans* (ATCC 10231) were considered to study the effect of the nanocomposites on their growth profiles. The former was cultured on Luria Bertani broth (LBB, HiMedia, India) by incubating 24 h at 37°C. Fresh culture of *C. albicans* was prepared in Potato Dextrose broth (PDB, HiMedia, India) and incubated for 48 h at 28°C.
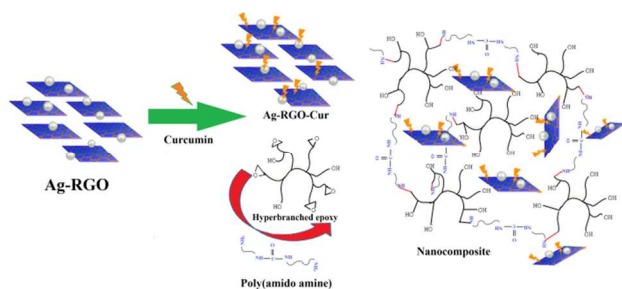
Fig. 1 Preparative protocol of the nanocomposite

Antimicrobial behavior of the nanocomposites against algae was investigated to determine their possible activity in marine coatings. The microalgal strain *Chlorella* sp. MP-1 (Genbank entry KJ499988) was cultured in Bold's Basal Medium (BBM) at 28±2°C with exposure to a light intensity of 1200 lux; photoperiod (14:10; light: dark cycle).

Minimum inhibitory concentrations (MIC) of the nanocomposites against the aforementioned microorganisms were evaluated by micro-dilution method as described elsewhere.[13] A stock solution of concentration 20 mg/mL was prepared by dissolving the nanocomposites in 1% DMSO. A series of concentrations were prepared by diluting the stock solution. 100 µL of samples with different concentrations were added into the wells of a 96 well plate. Two plates were taken this way and each of the microbial inoculum (*S. aureus* and *C. albicans*, each 100 µL) was added to the wells. The plates were incubated for 24 and 48 h respectively. After incubation, 40 µL of 3-(4,5-dimethylthiazol-2-yl)-2,5-diphenyltetrazolium bromide (MTT) solution was added to the wells and again incubated for 30 min. Characteristic blue color signifies the microbial growth, while inhibition can be predicted from no change in color.

Moreover, the efficacy of the nanocomposite thermosets was determined by monitoring the microbial growth profile in their presence. *S. aureus* and *C. albicans* were cultured in 15 mL test tubes in LBB and PDB broth. Tubes were incubated for 24 and 48 h respectively. Absorbance was taken at 600 and 620 nm to observe the absorbance variations in the growth profiles of the tested microorganisms. Similar test was also carried out for the microalgae, where it was cultured in BBM and kept for 15 days under observation.

Growth of microorganisms on the surface of a coating material hampers its longevity. Consequently, assays were carried out to examine their growth in the proximity of the nanocomposite surface. The bacterial and fungal strains (100 µL) were spread over solidified agar, while 500 µL (exponentially growing microalgal culture, 82×10^6 cells/mL) of the fresh microalgal suspension was spread over solidified BBM. A piece (1 cm × 1 cm × 0.25 mm) of the most effective nanocomposite was laid on the plates just before solidification. Plates were kept in an incubator for 24 and 48 h respectively for the bacteria and the fungi. The microalgal plates were incubated for 15 days under the aforementioned culture conditions as described in the previous section. Growth of microorganisms over the films was monitored by the images captured by a Nikon Coolpix-S3000 camera.

In vivo antimicrobial assay

S. aureus was considered as the representative microbe to
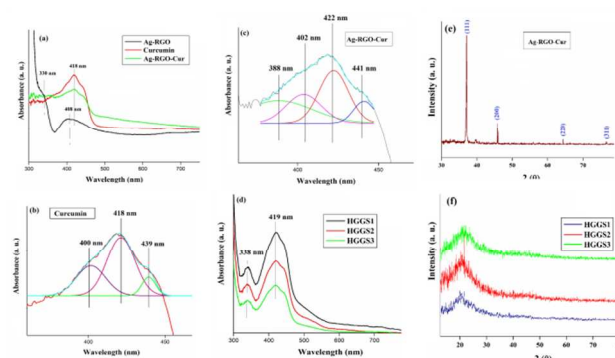
Fig. 2 (a) UV-visible spectra of cucumin, Ag-RGO and Ag-RGO-Cur, (b) Deconvulated spectrum of curcumin, (C) Deconvolated spectrum of Ag-RGO-Cur and (d) spectra of the nanocomposites and XRD patterns of (e) Ag-RGO-Cur and (f) the nanocomposites

ascertain the efficacy of the nanocomposite under *in vivo* condition. A 2 cm incision was made on the dorsal side of rats, which were divided into two groups (n=6, in each group). In one group, HGGS3 films were implanted and another group was closed as such by suturing. *S. aureus* inoculums (10^7 CFU/mL) was cultured overnight in LBB and applied to the surgical area of each group by swabbing with sterile cotton. After 24 h, moist cotton was used to swap the surgical area and it was dipped in LBB. The cotton was removed subsequently, after shaking the media with a vortex shaker. This was tested for CFU/mL count to ensure the total microbial colonies.[27]

After 3 days, the animals were sacrificed and a small portion was taken from the surgical area to analyze the presence of microbes. The skin sample was fixed in 2.5% gluteraldehyde solution and dehydrated in alcohol (70-100%). SEM micrographs were taken to see the inhibitory effect of HGGS3 on *S. aureus.*

Cytocompatibility of the nanocomposites

Cytotoxicity assay was performed for the nanocomposites by counting the viable cells (%). Wistar rat primary heart cells were taken for the test. Heart was extracted and cells were isolated using collagenase reperfusion procedure. They were cultured in low-glucose Dulbecco's modified Eagle medium (DMEM, Gibco Germany). Test materials were kept in the wells of a 96 well plate and the above culture was added into the wells. Wells without the film were taken as the control. The plate was incubated inside a CO_2 incubator at 37 °C for 24 h. Required amount of MTT was added to the wells followed by 8 h of incubation. Formazan crystals were formed, which were dissolved in DMSO and UV absorbance was recorded at 540 nm. Values of the absorbance were compared to that of the control to calculate the cell viability percentage.

Animals

Wistar rats (Male weighing 200-250 g) were taken from the Laboratory Animal Resources, Division of Pharmaceutical Technology, Defence Research Laboratory, Tezpur, Assam, India. Rats were kept under temperature range of 22–26 °C and 12 h of light-dark-alternative cycles. They were provided adequate nutrition and water *ad libitum*. Animal tests were carried out according to the Principles of LaboratoryAnimal care (NIH publication 85-23, revised 1985) with approval from the
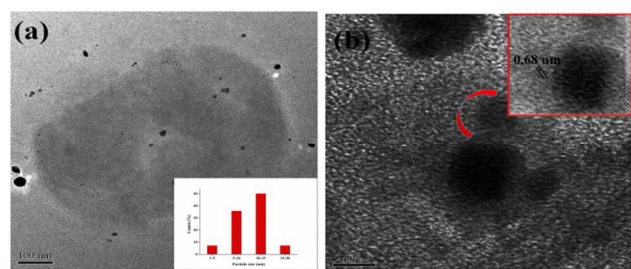
Fig. 3 HRTEM micrographs of the nanocomposite, Inset (a): histogram of distrbution of AgNP and Inset (b) An RGO sheet with lattice fringe spacing of 0.68 nm over AgNP

Institutional Animal Ethics Committee.

In vivo compatibility assessment

In vivo toxicity was assessed by implanting HGGS3 films (1 cm × 1 cm × 0.25 mm) subcutaneously into wistar rats (numbers,
5 n=6). Rats (n=6) without implants were kept as the control. Two vital factors of the implanted rats were taken under consideration, *viz*, blood parameters and histomorphological changes. For determining the former one, blood samples were collected at 0, 15 and 30 days of interval. Evaluations were done by using a
10 Coralyzer-100 automatic analyzer (Tulip Diagnostics, India) by following our recently reported method. Further, liver function, lipid and kidney profiles were tested by collecting the blood serum after 30 days of implantation.[13] For histomorphological study, fine sections of the organs (heart, kidney, liver and skin)
15 were prepared using a microtome. Sections were stained with hematoxylin and eosin (HE) followed by scrutiny under microscope.

Statistical Analysis

Data were analyzed and presented as mean±SD from the triplicate
20 results. ANOVA was done to understand real deviations amongst the results of the assays carried out to determine the MIC (two-way) and cytocompatibility (one way). Least significant difference (LSD) test was performed to determine the significant differences amongst the data.

25 # Results and discussion

Preparation of the nanocomposite

Plant extract mediated reduction of metal salts has attained great interest in the ever developing domain of nano-biotechnology.[28] In the present case, we adopted our recent protocol to prepare the
30 Ag-RGO.

Table 1: Study of curing and mechanical behavior

Property	HGGS1	HGGS2	HGGS3	LSD
Curing time at 120 °C (min)	22.6±1.5	20.6±0.57	17.5±0.5	0.81
Swelling (%)	25.1±0.7	30±1	23±1	0.76
Tensile strength (MPa)	54.3±0.5	59.6±0.45	65.5±0.3	0.35
Elongation at break (%)	21.7±0.6	19.2±0.26	17.7±0.45	0.38
Impact resistance (m)	>1	>1	>1	-
Scratch hardness (kg)	>10	>10	>10	-
Bending (mm)	<1	<1	<1	-
Adhesive strength (MPa) (wood)[a]	1410±2	2328.6±2.5	3370.6±2.5	31.23
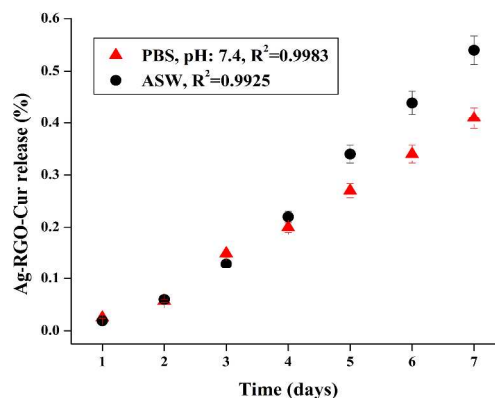
Fig. 4 Cumulative release profiles of Ag-RGOCur

Role of polyphenolic compounds in the simultaneous reduction
35 process was well depicted in that report.[13] Here, our interest was drawn by the immobilization of curcumin to Ag-RGO. Its structure possesses aromatic and aliphatic unsaturation, which helps to interact with the RGO by π- π electronic stacking. Thus, it holds a strong binding with Ag-RGO. Ultrasoniaction is an
40 efficient 'green' tool for immobilization of biomolecules onto nanomaterials. The immobilized system again interacts with the hyperbranched epoxy matrix with the surface hydroxyl functionalities and by π-electron affinity. This provides adequate stability to the nanocomposites which would be reflected in their
45 performance in regard of mechanical attributes and antimicrobial efficacy. The preparative scheme of the nanocomposite is presented in Fig. 1.

Nanocomposites were crosslinked at 120 °C and their curing times are given in Table 1. The curing time decreases with the
50 loading of the nanohybrid for the nanocomposites. Hyperbranched epoxy involves in a curing reaction with the amine hardener, by opening up the oxirane ring in presence of the

labile proton from the hardener. Moreover, hydroxyl groups of
55 curcumin may also take part in the process. That is why the aforesaid linear relationship was evidenced. All the nanocomposites showed adequate crosslinking (between 70-80%) which was observed by the swelling values (Table 1).

Characterization

60 UV-visible spectrum of bare curcumin showed a broad peak at around 418 nm (Fig. 2a), which upon deconvulation split to three peaks at 400, 418 and 439 nm (Fig. 2b,c). Characteristic peaks at 408 and 330 nm were observed for Ag-RGO (Fig. 2).[13] The second peak is due to the n-π* electronic transitions of the
65 aromatic carbon bonds of RGO. In case of the Ag-RGO-Cur, the total peak area was broadened. This upon deconvulation shows four peaks at 388, 402, 422 and 441nm. The surface plasmon peak of AgNP in Ag-RGO-Cur showed a blue shift from 408 to 388 nm, which is because of the oxygeneous groups present in
70 the curcumin structure.[29] This clearly indicates the interaction of curcumin with Ag-RGO. Similarly the presence of peaks at 338 and 419 nm indicates the presence of Ag-RGO-Cur in the nanocomposites (Fig. 2d).
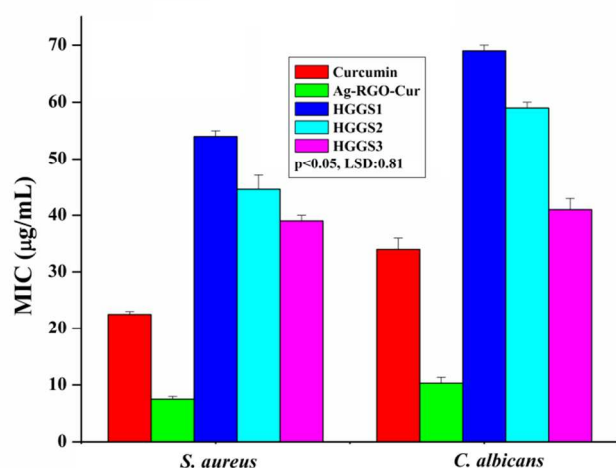
Fig. 5 MIC of the nanocomposites against bacteria and fungi

Fig. 6 Inhibition of growth of (a) Bacteria, (b) Fungus and (c) Microalga in presence of the nanocomposite

In the FTIR spectrum of curcumin, vitals bands were observed at 3420, 1623, 1510, 1286, 1137 and 1033 cm^{-1}. These correspond to the –OH, -C=O, -C-H, C-O groups of curcumin (ESI Fig. 1).[30] This confirms the successful extraction of curcumin from turmeric. All these bands are also present in other spectra (ESI Fig. 1) which confirmed the presence of curcumin in the immobilized nanohybrid as well as in the nanocomposite. In case of Ag-RGO-Cur, two characteristic bands were observed at 2871 and 2919 cm^{-1}, which are due to the symmetric and asymmetric vibrations of –CH- groups of the polyphenolic compounds of the plant extract. In the region 3300-3450 cm^{-1}, a broad band was observed which is attributed to the –OH stretching of curcumin and other polyphenolic compounds. Presence of the characteristic bands for oxirane ring at around 915–839 cm^{-1} confirms the epoxy groups in the nanocomposite. Contrarily, their absence proves the successful crosslinking of the nanocomposite by reacting with the poly(amido amine).

XRD pattern of Ag-RGO-Cur shows distinct peaks of silver at 2θ value 37.8, 44.9, 64.2 and 76.4° that represents the face-centered cubic structure of silver (JCPDS 89-3722), with corresponding Bragg's reflection planes (111), (200), (220) and 311) (Fig. 2e,f). Literature reports the crystalline nature of curcumin.[31] However, Ag-RGO-Cur did not show distinct crystalline peaks. Interaction with the nanohybrid as well as low amount of it is attributed to this fact. Amorphous nature of hyperbranched epoxy was witnessed by the broad peaks at around 2θ=20-22° in the nancomposites.

TEM micrographs of the nanocomposites are presented in Fig. 3. Narrow size distribution of AgNP was clearly visible from the histogram, where maximum particles lie between of 10-15 nm. Moreover these particles are embedded within the RGO sheets. Again, Ag-RGO was distributed in the hyperbranched epoxy matrix. An RGO sheet with lattice fringe spacing 0.68 nm was observed over AgNP. This indicated that the nanomaterials have efficient interaction between them and the nanohybrid is strongly interacting with the epoxy matrix. The π-π electron affinity plays the vital role in this case. These types of interactions lead to the enhancement of mechanical attributes in nanocomposites.

Performance of the nanocomposites
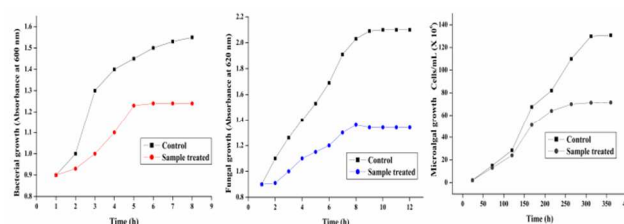
Literature reports that graphene epoxy nanocomposite exhibited augmentation of mechanical properties.[21] Table 1 reveals increment of tensile strength of the nanocomposite with the increase in loading of Ag-RGO-Cur. Layered RGO sheets embedded with AgNP improved the interfacial interaction with the hyperbranched epoxy matrix. As a result, this enhancement of the tensile strength was witnessed. Loading of Ag-RGO-Cur however, restricts the epoxy chains due to which elongation at break gets decreased. Beyond this level of loading, phase separation was observed after the nanocomposites were cured. Flexibility of epoxy is a major concern for the researchers. The nanocomposite films could be folded up to a curvature of 180°, without any fracture. Values of scratch hardness and impact resistance were above the instrumental limits (Limits of the instruments: impact resistance=1 m, scratch hardness=10 kg). Thus, considering the mechanical attributes, HGGS3 can be said the best performing nanocomposite.

Similar increment was also observed in case of the lap sheer tensile adhesive strength of the thermosetting nanocomposites. Surface functional groups of the hyperbranched epoxy and the wood substrates interact extensively. As a result linear increment was observed with the Ag-RGO-Cur loading. Mechanical and adhesive properties set evidence that the prepared nanocomposites are suitable for their utility in advanced applications. Aiming at the aforesaid objectives, the present work calls for a scrutiny of biocompatibility and antimicrobial activity of the material. The data presented in Table 1 are significantly different in case of the three nanocomposites, with p value<0.05.

Release of Ag-RGO-Cur

For attractive service performance, sustained release of the active components is essential for an antimicrobial material. This test was carried out to sketch the release profiles of Ag-RGO-Cur under *in vitro* physiological conditions (PBS, pH: 7.4) as well as under marine condition (ASW). Extensive crosslinking of the thermosetting nanocomposite and good physicochemical interactions amongst the components allowed very slow release of Ag-RGO-Cur. Thus, in both the cases, no detectable release was witnessed before 24 h (Fig. 4). Hence, the experiments were carried out for 7 days to measure the leaching percentage. Only 0.41±0.02 (in PBS, pH: 7.4) and 0.54±0.03% (in ASW) of the components released out from the nanocomposite after 7 days under experimental conditions. In the real field of application it is expected to show a sustained release profile for a significant service life. However, the relative rate of release was faster under marine condition. This kind of release profile is useful in biomedical domain for designing infection resistant surfaces. Moreover, their activity can also be utilized to fabricate high
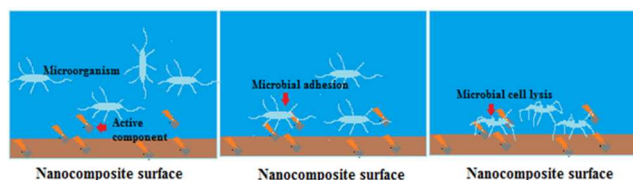
Fig. 7 Probable mechanism of the antifouling activity of the nanocomposite

performance, sustained released marine coatings.

Antimicrobial activity against bacteria, fungi and algae

MIC was calculated for the nanocomposites against *S. aureus* and *C. albicans* (Fig. 5). Our previous report demonstrated enhanced inhibitory effect of Ag-RGO over the individual components.[13] In that report, Ag-RGO showed MIC against *S. aureus* and *C. albicans* at 12.5 and 16 µg/mL. Here, these values were reduced to 7 and 10 µg/mL respectively, which showed clear enhancement of antimicrobial activity upon immobilization of curcumin to Ag-RGO. Curcumin is a renowned antimicrobial agent found abundantly in nature. Again, immobilization of biomolecules onto the nanomaterial surface increases its efficacy by synergistic effect at bio-nano-interface.[32] Antimicrobial activity of a material depends on its surface structure. Ag-RGO provides a high surface area, which complemented the activity of curcumin. However, in case of the nanocomposites, lower MIC values were observed, which can be attributed to the indirect exposure of the active components to the microbes. Additionally, the significant reduction of the nanohybrid amount with respect to the matrix is also responsible for the above findings. Profound antimicrobial activity was witnessed with increase in the amount of Ag-RGO-cur in the nanocomposites. HGGS3 showed MIC at 38 and 41µg/mL against the bacterium and the fungus respectively. Thus, this could be clearly understood that the nanocomposite could sufficiently inhibit bacterial and fungal fouling at 3 wt% loading of Ag-RGO-Cur within it. However, it is expected that the active components can be leached out with due course of time and antimicrobial action will be sustained as evident by the aforementioned assays. Statistically significant differences were found in the MIC assay, with LSD: 0.81 and p values<0.05.

Again, Fig. 6 indicates clear decrement of the microbial growth with time when incubated with the nanocomposite (HGGS3). Absorbance of *S. aureus* shows exponential growth with time in case of control. On the other hand, their growth decreases and come to a steady state in presence of the nanocomposite. This ascertains that the nanocomposite possesses antibacterial properties.   Similar absorbance profile was witnessed for *C. albicans* in presence of the nanocomposite film. The active component may leach out very slowly which could interact with the microorganisms and cause damage to their cellular organization. Further, adherence of microbes to the nanocomposite surface causes microbial cell lysis, which leads to a decrease in their population and stops their further growth.[33] This type of activity is essential for an antimicrobial material, which could prevent infection at surgical sites, by following the aforementioned mechanism (Fig. 7).

Unlike bacteria and fungi, the growth of microalgae was not monitored spectrophometrically. The microalgal growth was
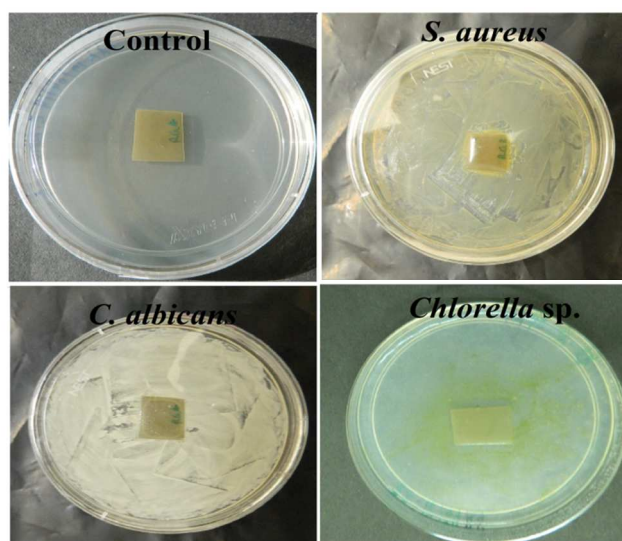
Fig. 8 Antimicrobial activity of the nanocomposites in the proximities of bacteria, fungi and microalgae

monitored by measuring the cell concentration in a Neubauer haemocytometer (in triplicates) at regular intervals of 48 h for 15 days. From Fig. 6, a gradual progressive decline in microalgal growth is evident. This may be attributed to the fact that the microalgae could not adhere to the nanocomposite surface and deposited at the bottom of the test tubes, whereby demonstrating competitive growth inhibition.[34] Additionally, the light absorbing capacity of RGO may also help in prevention of microalgal growth.[35] Hence, the present nanocomposite has the potential to provide a surface that could prevent microalgal growth upon its surface. Marine coatings with such properties may help in resisting the growth of different fouling microalgae.

Moreover, assays were carried out to examine the possibility of microbial growth in the proximity of the nanocomposite. Fig. 8 shows clear evidence that neither the bacteria nor the fungi could grow on the surface of the nanocomposite within an area of 1 cm². On the other hand, their uniform growth is visible throughout the rest parts of the plates. Although the microalgal growth is not uniform, no growth is seen on the surface of the nanocomposite within an area of 1 cm².

Thus, the aforesaid assays confirmed that the nanocomposite could prevent the growth of the two most notorious microorganisms responsible for causing infection at surgical sites. This may be utilized to design protective coatings for surgical implants and devices. Moreover, the surface was able to inhibit microalgal fouling over it, which may endorse the same material for utilization in advanced marine coatings. However, in both the cases, toxicity of the materials should be analyzed properly.

***In vivo* antimicrobial assay**

Visually, no infection was evident in the HGGS3 implanted rats, while un-implanted rats faced severe infection (Fig. 9). Acute edema and erythema were visible in the infection area of the latter group. This clears the microbial infection resistance ability of HGGS3, which is a very important criterion for implantable biomaterials.[36] Further, colonies recovered from the animals were presented in ESI Table 1. It was observed that bacterial colonies were decreased with time in HGGS3 implanted rats.
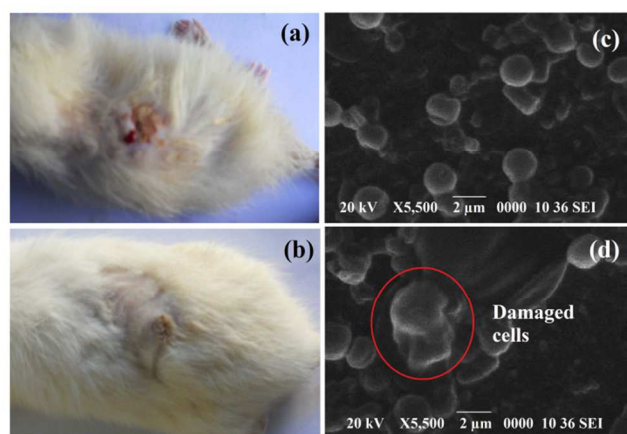
Fig. 9 (a) Severe infection on un-implanted rat, (b) No sigh of infection on HGGS3 implanted rat and SEM micrographs of (c) Un-implanted skin, (d) Implanted skin

Again, SEM micrographs of the un-implanted sample showed abundant growth of *S. aureus* without losing cellular integrity. Contrarily, disruption, morphological alteration and agglomeration of bacterial cells were seen in case of the HGGS3
5 implanted rats.

Above assays thus confirmed the antimicrobial efficacy of the material under *in vitro* as well as *in vivo* conditions.

Cytocompatibility assessment

To examine the *in vitro* toxicity of the material, mammalian
10 primary heart cells were considered. RGO showed 72% compatibility with the cells (Fig. 10). Upon formation of Ag-RGO this was increased to 83.2%. Again, immobilization of curcumin increased this value to 84.7%, where content of curcumin was 33%. We previously observed the compatibility of
15 Ag-RGO with mammalian peripheral blood mononuclear cells (PBMC) and red blood cells (RBC).[13] Further, curcumin is a common ingredient of regular food items. Therefore, Ag-RGO-Cur was expected to show good compatibility with mammalian cell lines (with 66% of Ag-RGO and 33% of curcumin in the
20 system). The hyperbranched epoxy again possesses good biocompatibility with its glycerol based architecture. Thus, the nanocomposites demonstrated more than 89% cell viability, where content of curcumin varies from 0.016 to 0.049 g respectively for HGGS1 to HGGS3. Only subtle difference was
25 observed in the three nanocomposites, due to small scale loading of Ag-RGO-Cur. Significant difference was witnessed among survival percentages of treatments ($p < 0.05$ and LSD: 0.45).

Table 2: Liver function, kidney and lipid profiles of the implanted rats with the control

Parameters	Control	HGGS3
Low density lipoprotein (mg/dL)	115.8±0.5	118.1±0.81
High density lipoprotein (mg/dL)	47.2±0.80	46.5±0.27
Cholesterol (mg/dL)	39.2±0.32	35.3±0.37
Triglycerides (mg/dL)	9.2±0.2	8.7±0.15
Glucose (mg/dL)	112.5±0.25	110.6±0.2
Urea (mg/dL)	70.7±0.41	69.7±0.35
Total protein (g/dL)	5.7±0.15	6.3±0.5
Uric acid (mg/dL)	1.14±0.05	1.74±0.03
Alanine aminotransferase (U/L)	78.7±0.45	75.5±0.4
Aspartate aminotransferase (U/L)	110.6±0.3	112.3±0.45
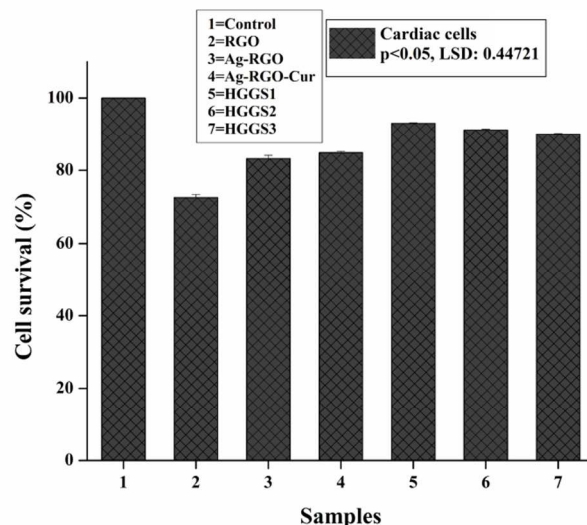
Fig. 10 Cell viability (%) of the primary cardiac cells

30 This assay ascertained the cytocompatibilty of the prepared nanocomposites, which is a primary criterion for a material to be used in biomedical applications. However, for actual endorsement of such materials to the real field, *in vivo* compatibility assessment is a prerequisite.

35 ***In vivo* compatibility assessment**

Hematological parameters regulate different physiological functions of the body. Change in their values from the normal range may cause heavy damage to the body. Therefore, it is important to check these parameters after implantation of a
40 biomaterial into the host body. ESI Table 2 gives a clear picture of the hematological parameters of the nanocomposite implanted rats which are nearly comparable to that of the control rats. However, the parameters suggested initial marginal increment (up to 15 days) in the level of macrophage (matured monocytes),
45 neutrophil or lymphocytes, which is due to the surgery and introduction of the foreign polymeric nanocomposite. But, their gradual normalization after 15 days, indicated the immunocompatibility of this material within the host body.

Further, lipid, kidney profiles and liver function of the
50 implanted rats were determined and compared with the control parameters, by analyzing the serum biochemistry of their blood. Lipid profile (LDL, HDL, Chol and TGL) can help in screening the abnormality of body lipids which can lead to cardiovascular disorder.[37] Again, ALT/SGPT and AST/SGOT are the
55 biomarkers of animal liver function. Table 2 shows comparable results of lipid profile and liver function test values of the implanted and the control rats. Besides, Gluc, urea, UA and Cre values confirms no induction abnormality in the kidney profiles of the rats after implantation of the nanocomposite (Table 2).

60 These findings were further validated by the histopathlogical studies of the treated rats (ESI Fig. 2). Skin was taken from the area near the implant. On 7th post implantation day, disrupted striated skin muscles were seen. However, no infiltration of immune cells was visible, which is supported by the
65 haematological parameters. The figure also shows the skin sections on 15th and 30th days from implantation. Different epithelial layers are clearly visible in the representative skin

section. Also, the absence of any capsule formation suggested good integration of the material with the surrounding tissues.[38] Similarly, liver and kidney sections represent normal cellular organizations like the hepatocytes and the glomerulus etc. Heart
5 section was observed with regular nuclei and intercalated discs.

In vivo findings demonstrated the potential utility of the nanocomposite in the field of biomedical applications, as an efficient thin film material over implant devices. Further, this also ascertains the compatibility of the nanocomposite with the higher
10 aquatic animals dwelling in the sea. Moreover, a comparative account of the state of art reported antimicrobial/antifouling materials with the present material is included in the ESI Table 3 to understand the superiority of the latter.

Conclusion

15 An efficient biocompatible material based on hyperbranched epoxy nanocomposite is put forward in the present study for advanced antimicrobial applications. Properties of Ag-RGO were complemented by the immobilization of a naturally abundant biomolecule, curcumin. The nanocomposite inhibited bacterial,
20 fungal and algal growth on its surface. Moreover, *in vitro* and *in vivo* assays confirmed the biocompatibility of the material with mammalian hosts. Present findings suggest the potential of the nanocomposite as a thin film material in the domain of biomedical implants and devices. Further, the properties of the
25 same material could be utilized to design a microbial fouling resistant marine coating. However, field assays are required to be carried out before their actual use.

Acknowledgements

40 Notes and references

ªAdvanced Polymer and Nanomaterial Laboratory, Department of Chemical Sciences, Tezpur University, Napaam-784028, Assam, India
ᵇDefence Research Laboratory, Tezpur, Assam, India
ᶜDepartment of Molecular Biology and Biotechnology, Tezpur University,
45 *Napaam- 784028, Assam, India*

1 L. Xiao, J. Li, S. Mieszkin, A. Di Fino, A. S. Clare, M. E. Callow, J. A. Callow, M. Grunze, A. Rosenhahn and P. A. Levkin, ACS Appl. Mater. Interfaces, 2013, 5, 10074.
50 2 A. Statz, J. Finlay, J. Dalsin, M. Callow, J. A. Callow and P. B. Messersmith, Biofouling, 2006, 22, 391.
3 A. Roosjen, H. C. Van Der Mei, H. J. Busscher and W. Norde, Langmuir, 2004, 20, 10949.
4 C. Perrino, S. Lee, S. W. Choi, A. Maruyama and N. D. Spencer,
55 Langmuir, 2008, 24, 8850.
5 K. Schiff, D. Diehl and A. Valkirs, Marine. Poll. Bull. 2004, 48, 371.

6 S. Silver, L. T. Phung and G. Silver, J. Ind. Microbiol. Biotechnol. 2006, 33, 627.
7 S. Barua, R. Konwarh, S. S. Bhattacharya, P. Das, K. S. P. Devi, T. K.
60 Maiti, M. Mandal and N. Karak, Colloids Surf., B, 2013, 105, 37.
8 S. Agnihotri, S. Mukherji and S. Mukherji, RSC Adv. 2014, 4, 3974.
9 M. Roy, P. Mukherjee, B. P. Mandal, R. K. Sharma, A. K. Tyagi and S. P. Kale, RSC Adv. 2012, 2, 6496.
10 S. Barua, R. Konwarh, M. Mandal, R. Gopalakrishnan, D. Kumar and
65 N. Karak, Adv. Sci. Eng. Med. 2013, 5, 291.
11 P. Dallas, V. K. Sharma, R. Zboril, Adv. Colloid Interface Sci. 2011, 166, 119.
12 S. Zhang, K. Yang, L. Feng and Z. Liu, Carbon, 2011, 49, 4040.
13 S. Barua, S. Thakur, L. Aidew, A. K. Buragohain, P. Chattopadhyayc
70 and N. Karak, RSC Adv. 2014, 4, 9777.
14 R. De, P. Kundu, S. Swarnakar, T. Ramamurthy, A. Chowdhury, G. B. Nair and A. K. Mukhopadhyay, *Antimicrob. Agents Chemother.* 2009, 53, 1592.
15 G, Reusmann, Macromol. Symp. 2002, 187, 235.
75 16 S. Barua, G. Dutta and N. Karak, Chem. Eng. Sci., 2013, 95,138.
17 B. De and N. Karak, J. Mater. Chem. A, 2013, 1, 348.
18 S. Barua, N. Dutta, S. Karmakar, P. Chattopadhyay, L. Aidew, A. K. Buragohain and N. Karak, Biomed. Mater. 2014, 9, 025006 (14pp).
19 D Ratna, O Becker, R Krishnamurthy, G. P. Simon and R. J. Varley,
80 Polymer, 2003, 44, 7449.
20 B. Roy, P. Bharali, B. K. Konwar and N. karak, Bioresour. Technol. 2013, 127, 175.
21 X-J Shen, Y. Liu, H-M Xiao, Q-P Feng, Z-Z Yu, S-Y Fu, Compos. Sci. Technol. 2012, 72, 1581.
85 22 S-Yi Yang, W-N Lin, Y-L Huang, H-W Tien, J-Yu Wang, C-C M. Ma, S-M Li and Y-S Wang, Carbon, 2011, 49, 793.
23 L. P. Almeida, A. P. F. Cherubino, R. J. Alves, L. Duffosé and M. B. A. Glória, Food Res. Int. 2005, 38, 1039.
24 D. R. Dreyer, S. P.ark, C. W. Bielawski and R. S. Ruoff, Chem. Soc.
90 Rev. 2010, 39, 228.
25 J. A. Berges and D. J. Franklin, J. Phycol. 2001, 37, 1138.
26 I. M. El-Sherbiny and H. D. C. Smyth, Mol. Pharmaceutics 2012, 9, 269.
27 A. M. Elsome, J. M. T. Hamilton-Miller, W. Brumfitt, W. C. Noble, J.
95 Antimicrob. Chemother. 1996, 37, 911.
28 T.N.V.K.V. Prasad and V.S.R. Kambala and R.A. Naidu, Curr. Nanosci. 2011, 7, 531.
29 V. G. Pol, D. N. Srivastava, O. Palchik, V. Palchik, M. A. Slifkin, A. M. Weiss and A. Gedanken, Langmuir 2002, 18, 3352.
100 30 D. Brahatheeswaran, A. Mathew, R. G. Aswathy, Y. Nagaoka, K. Venugopal, Y. Yoshida, T. Maekawa and D. Sakthikumar, Biomed. Mater. 2012, 7, 045001 (16pp).
31 A. Sahu, N. Kasoju, P. Goswami and U. Bora, J. Biomater. Appl. 2011, 25, 619.
105 32 S. Liu, L. Wei, L. Hao, N. Fang, M. W. Chang, R. Xu, Y. Yang and Y. Chen, ACS Nano, 2009, 12, 3891.
33 M. L. W. Knetsch and L. H. Koole, Polymers, 2011, 3, 340.
34 C. W. Y. Lam, W. B. Silvester, Hydrobiologia, 1979, 63, 135.
35 X. Bai, Y. Zhai and Y. Zhang, J. Phys. Chem. C 2011, 115, 11673.
110 36 B. Das, M. Mandal, A. Upadhyay, P. Chattopadhyay and N. Karak, 2013, 8, 035003.
37 J Santos, Int. J. Std. AIDS, 2005, 16, 677.
38 E. A. Deitch, A. A. Marino, V. Malakanok and J. A. Albright, 1987, 27, 301.